THE PENNSYLVANIA STATE UNIVERSITY
SCHREYER HONORS COLLEGE

DEPARTMENT OF ENGINEERING SCIENCE AND MECHANICS

PRECIPITATION HEAT TREATMENT OF LASER DIRECTED ENERGY DEPOSITION ADDITIVE MANUFACTURED TI-RICH NITI SHAPE MEMORY ALLOYS

JESSICA MACAULEY SPOLL
SPRING 2016

A thesis
submitted in partial fulfillment
of the requirements
for a baccalaureate degree
in Engineering Science
with honors in Engineering Science

Reviewed and approved* by the following:

Reginald Hamilton
Professor of Engineering Science and Mechanics
Thesis Supervisor

Bruce Gluckman
Professor of Engineering Science and Mechanics
Honors Adviser

Judith Todd
P. B. Breneman Department Head Chair

* Signatures are on file in the Schreyer Honors College and Engineering Science and Mechanics Office.

Abstract

This research investigates additive manufacturing as a fabrication method for shape memory alloys. Shape memory alloys (SMAs) undergo a reversible solid-state martensitic phase transformation that results in high recoverable strains, making them useful in industrial applications. NiTi alloys are widely used SMAs. However, due to their sensitive material properties, micromachining fine features in NiTi materials is difficult. Additive manufacturing (AM) allows for complex 3D geometries to be fabricated directly to the final dimensions, albeit surface finishing may be required. Moreover, AM has the capability to design material microstructures “on demand” by controlling input feedstock composition and deposition parameters during fabrication. This opens up avenues for manufacturing gradient microstructures for functionally graded materials.

For this research, Ti-rich builds were fabricated using the additive manufacturing technique of laser directed energy deposition. The feedstock was elementally blended Ni and Ti powders and resulted in a $Ti_{53.1}Ni_{46.9}$ at.% build. Previous results from the Hamilton group showed that laser directed energy deposition additive manufactured (LDEDAM) Ni-rich NiTi alloys had an anisotropic microstructure in the as-deposited condition. The degree of anisotropy was reduced using precipitation heat treatment. For LDEDAM Ti-rich NiTi alloys in the as-deposited condition, previous work showed the thermal-induced martensitic phase transformation (TIMT) occurred at temperatures higher than those for the Ni-rich compositions. Thus, the Ti-rich material is attractive for applications requiring the shape memory effect above room temperature.

This work builds upon the Hamilton group's previous work on as-deposited LDEDAM Ti-rich NiTi alloys. The goal of this research is to investigate the influence of precipitation heat treatment on the transformation temperatures of the as-deposited material condition. Two different durations are used at one precipitation heat treatment temperature. Differential scanning calorimetry (DSC) experiments are used to measure characteristic phase transformation temperatures and enthalpies. Samples for calorimetry analysis were micromachined from different height locations within the LDEDAM build in order to spatially resolve the behavior, as the layer-by-layer fabrication is expected to cause microstructure anisotropy for the Ti-rich NiTi alloys. The results from DSC analysis show that the transformation temperatures for the precipitation heat treated material are comparable to the as-deposited material. The enthalpy measurements for the TIMT on cooling and heating become equivalent for the longer duration precipitation heat treatment. Ultimately, the results show that precipitation treatments may improve the reversibility of the TIMT without altering the operating temperature ranges.

Table of Contents

List of Figures

List of Tables

Acknowledgments

First, I would like to thank my thesis advisor, Dr. Reginald Hamilton, for the opportunity to work on this project. I would also like to thank Beth Last, Ph.D. candidate, for her support and guidance. This work would not have been possible without her. I also want to thank my friends and family for supporting me while writing this thesis and always being there for encouragement. Special shout-out to Amel, Maggie, and Manuel for bringing me happiness every day.

Chapter 1
Introduction

Shape memory alloys (SMAs) are metallic alloys that can “remember” their previous form and revert back to it after being subjected to thermomechanical variations. There are two important material responses of SMAs that give them the ability to recover large deformations: the shape memory effect and the pseudoelastic effect. For the shape memory effect (SME) deformation is recovered via heating, and for the pseudoelastic effect (PE) it is recovered during unloading [1]. SMAs are useful in different applications because of this behavior. One application that is familiar to many people is eyeglasses that can bend and then return to their original shape [2]. SMAs are ideal for medical applications as well. A wire in its deformed state will have a small enough cross-section to be introduced easily into an artery, and once it is in place it can return to its original shape after being triggered by body heat [3]. To date, more than 10,000 United States patents and over 20,000 worldwide patents have been issued on SMAs and their applications [1]. Due to its superior mechanical properties, NiTi-based alloys are the most important of the known SMAs and are the focus of this research.

Due to the high ductility and elasticity of NiTi, it is difficult to create intricate shapes during machining processes [4]. To mitigate this issue, near net-shaping fabrication methods have been investigated, including additive manufacturing [5]. During additive manufacturing (AM), parts are fabricated by melting layers of metallic powder and adding layers on top of each other. Using

AM, the poor machinability of NiTi is overcome since it enables the production of complex 3D geometries. This thesis focuses on the use of laser-based directed energy deposition technology to fabricate NiTi specimens. Directed energy deposition was chosen to create these specimens because elementally blended powders could be used. Different ratios of nickel and titanium can be created from elementally blended Ni and Ti powders. This research focuses on Ti-rich specimens.

AM is a new fabrication approach for NiTi. Past research has shown that the directed energy deposition AM technique can cause anisotropy in the microstructure. Since the unique material properties of NiTi depend on the microstructure, this is not ideal. The anisotropy may result from the exposure of the layers to complex thermal histories as layer upon layer is deposited [6]. Previous work from the Hamilton group report spatial heterogeneity of the phase transformation temperatures throughout as-deposited builds of additively manufactured Ni-rich NiTi [6]. An anisotropic microstructure was confirmed in their more recent work.

Homogeneity of the microstructure is desired so that the unique properties of NiTi are uniform throughout the build. Homogeneity can be achieved through heat treatments. Solution treatments that heat the material at high temperatures for long times can produce a solid solution, with all secondary phases dissolved, that is homogeneous after rapid cooling. The objective of this research is to carry out post-deposition precipitation heat treatments for laser directed energy deposition additive manufactured (LDEDAM) Ti-rich NiTi alloys and spatially resolve stress-free thermal-induced phase transformation temperatures.

Chapter 2
Background on Shape Memory Alloys

Shape memory alloys are a class of metal alloys that can recover apparent permanent deformation when heated above a certain temperature or unloaded. This characteristic of SMAs has resulted in their use for a variety of applications in many fields. For instance, NiTI SMAs are widely used in the medical field because of their osseo-integration, super-elasticity, shape memory effect and biocompatibility [7]. Porous NiTi is preferred for bone scaffolds since its elastic modulus is more comparable to that of bone than of steel or Ti alloys and its weight is closer to that of the replaced bone [7]. Other examples of applications include their use as cell phone antennas, thermal and mechanical actuators, automotive devices, and helicopter blades.

2.1 NiTi

In 1963, William J. Buehler, a metallurgist at the Naval Ordnance Laboratory (NOL), discovered the properties of nickel titanium and named it Nitinol (NiTiNOL), combining the composition and the laboratory [8]. While the potential applications for Nitinol were understood at the time, commercialization took nearly a decade [2].

The NiTi-based alloys are the most commercially successful SMAs with excellent mechanical properties [9]. Phase transformations in the NiTi-based alloy system include

diffusionless/martensitic transformations, from which the shape memory behavior arises [9]. It is known that the Ni concentration in NiTi affects the phase transformation temperatures, such that the martensite start temperature (M_s) decreases with increasing Ni content [10]. NiTi-based alloys also exhibit low elastic modulus, corrosion resistance, abrasion resistance, high ductility, high strain recoverability, stable transformation temperatures, and high biocompatibility [11].

The focus of this thesis considers the thermal-induced phase transformation, which is the basis for the shape memory effect and the pseudoelastic effect. SMAs exhibit one stable phase at high-temperature called austenite, and another at low-temperature called martensite. The martensite can exist as twinned and detwinned, as shown in Figure 1 [12].

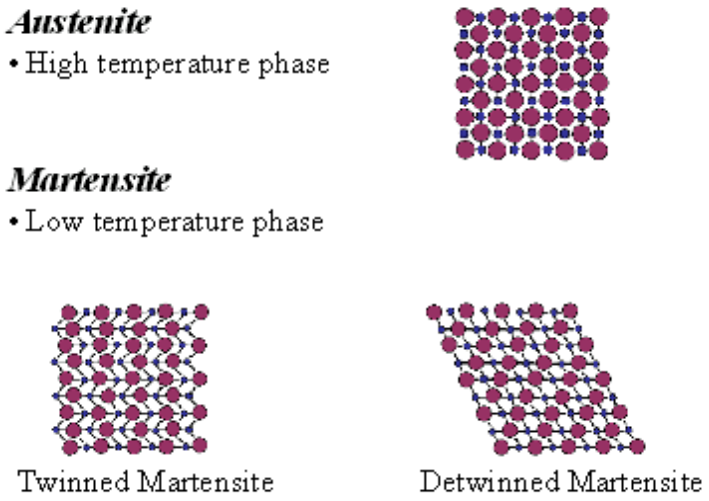

Figure 1: Different phases of a SMA (Taken from [11], used without permission)

A phase transformation between these two phases from heating or cooling is the cornerstone of the unique properties of SMAs: the shape memory effect and pseudoelasticity. Upon cooling, in the absence of an applied load, the material transforms from austenite into twinned martensite,

and no observable shape change occurs. Upon heating, the material transforms from martensite back to austenite. This transformation is defined by four characteristic temperatures, as shown in Figure 2: Martensitic start temperature (M_s), where the material starts transforming from austenite to martensite; martensitic finish temperature (M_f), where the transformation is fully in the martensitic phase; austenite start temperature (A_s), where the reverse transformation from austenite to martensite starts; and austenite finish temperature (A_f), where the material is fully in the austenite phase [12].

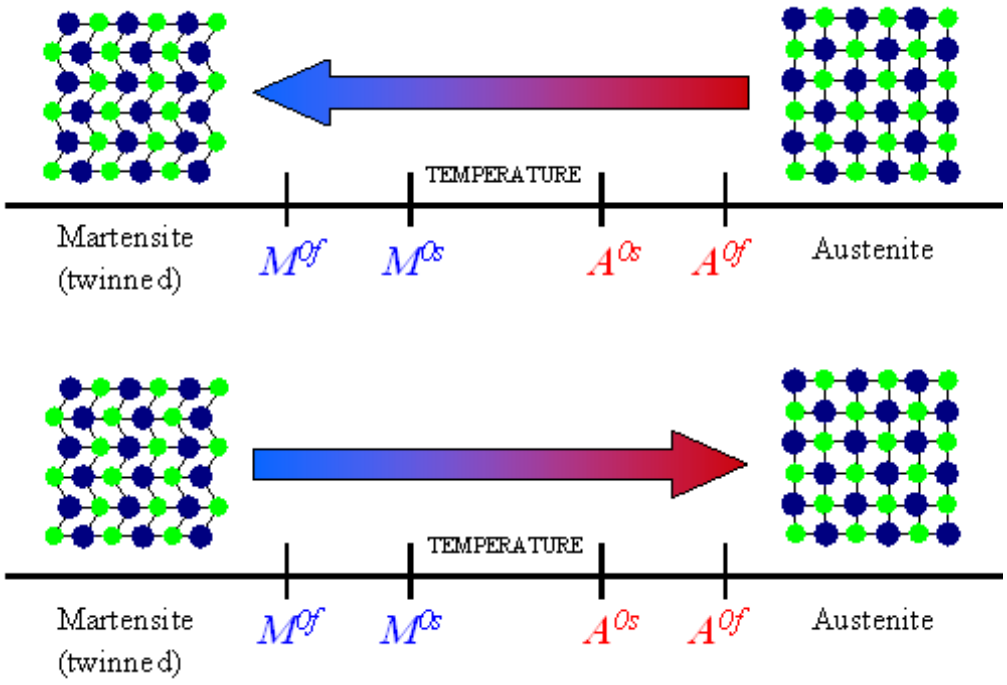

Figure 2: Temperature-induced phase transformation without mechanical loading. Taken from [12]**, used without permission.**

"Shape memory" refers to a plastically deformed material returning to its original shape upon heating. If a mechanical load is applied to the material while it is in the twinned martensitic phase at low temperatures, it is possible to detwin the martensite, and this results in a visible shape change. The deformed configuration is retained when the load is released (Figure 3). The

load applied must be sufficiently large to start the detwinning process [13]. Subsequent heating of the SMA at a temperature above A_f results in a reverse phase transformation from detwinned martensite to austenite and leads to complete shape recovery (Figure 4).

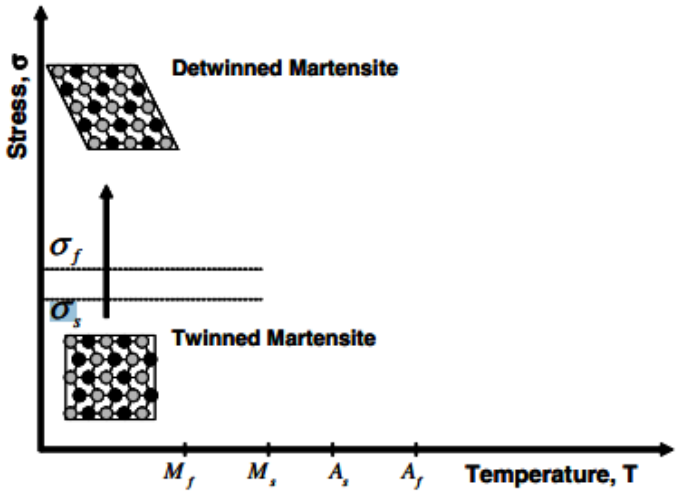

Figure 3: Schematic of shape memory effect of a SMA showing the detwinning of a material with an applied stress (Taken from [14]**, used without persmission)**

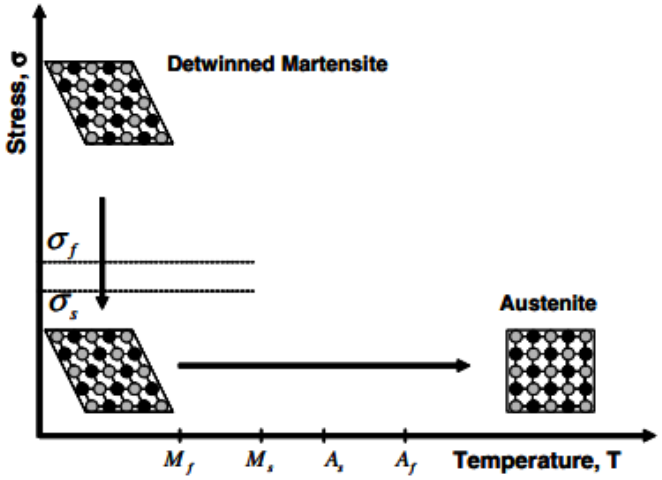

Figure 4: Schematic of shape memory effect of a SMA showing the unloading and subsequent heating to austenite under no load condition (Taken from [14]**, used without permission)**

The phenomenon is more specifically referred to as the one-way shape memory effect. Figure 5 depicts the overall shape memory effect [14].

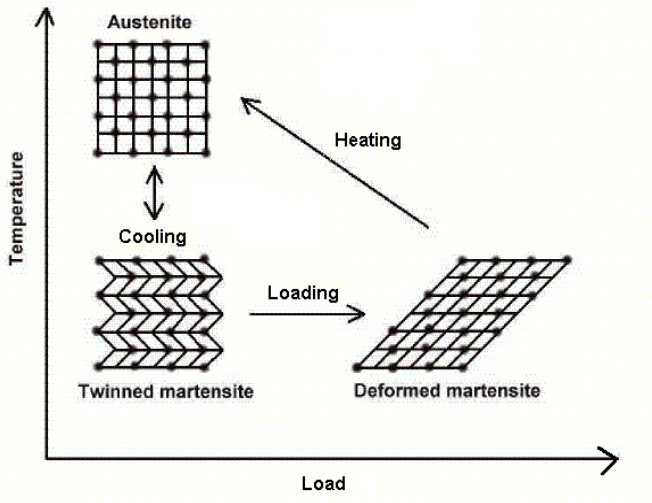

Figure 5: Transformation from the austenite to the martensite phase and the shape memory effect (Taken from [14]**, used without permission)**

The other unique property of NiTi is the pseudoelastic effect. The Pseudoelastic effect (PE) is induced by applying a mechanical load at constant temperature above the A_s temperature. The alloy is initially in the austenite phase. A very large strain is observed as a result of the load, which causes the austenite to transform into martensite. Upon unloading, complete shape recovery can occur as the material returns to the austenite phase. The effect is shown schematically in Figure 6 and the corresponding stress-strain diagram is shown in Figure 7 [12].

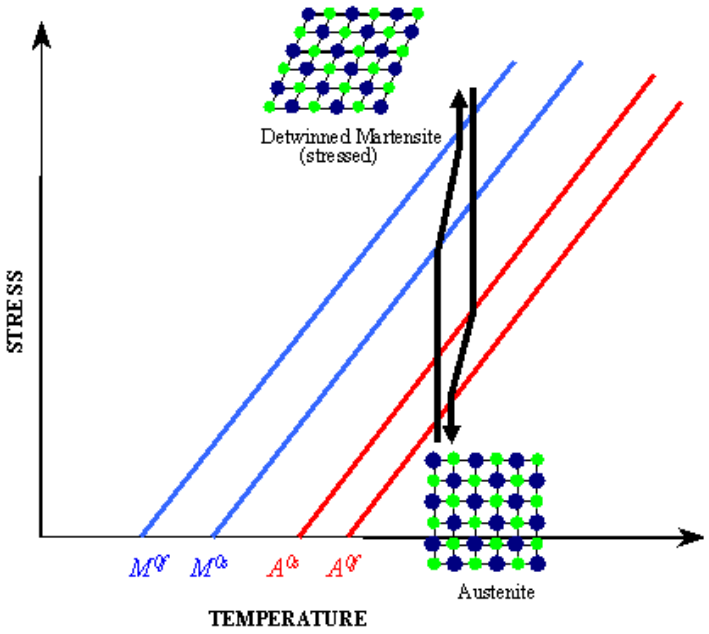

Figure 6: Pseudoelastic loading path (Taken from [12]**, used without persmission)**

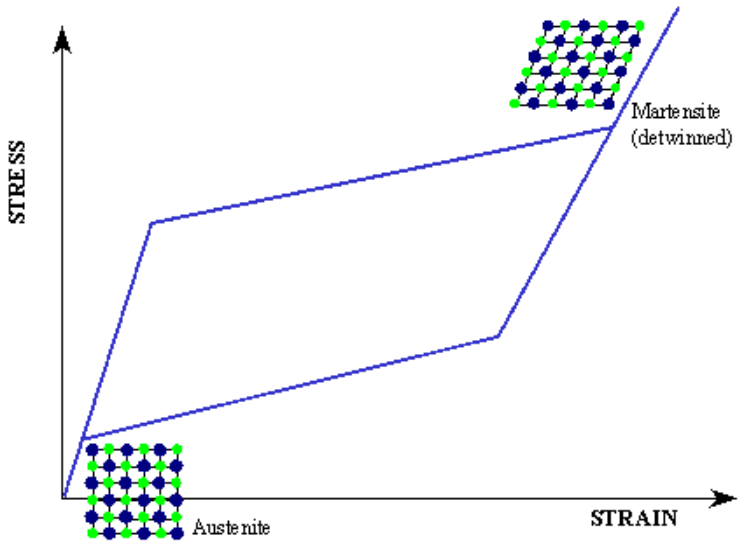

Figure 7: Pseudoelastic stress-strain diagram (Taken from [12]**, used without persmission)**

2.2 Ti-rich NiTi

The material specifically studied in this thesis is a titanium (Ti) rich NiTi alloy composition. This indicates that the composition was more than 50 atomic percent (at. %) Ti, with the balance being nickel (Ni). The phase diagram of the Ti-Ni system is given in Figure 8 [10]. In this figure, 1257 K is the temperature at which NiTI is in solid solution. The dashed line between the arrows shows the range of possible NiTi compositions.

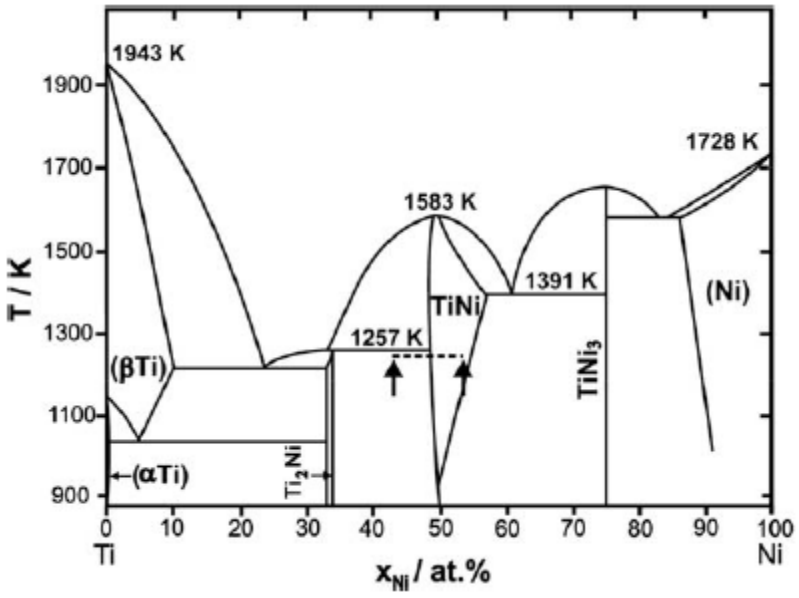

Figure 8: Phase diagram for Ti-Ni system (Taken from [10]**, used without permission)**

As mentioned earlier, the M_s temperature sharply decreases with increasing Ni content based on empirical data [10]. The M_s temperature will be relatively high for Ti-rich compositions. This is depicted in Figure 9 for Ni concentrations (X_{Ni}) less than 50 at. %, which fall in region I.

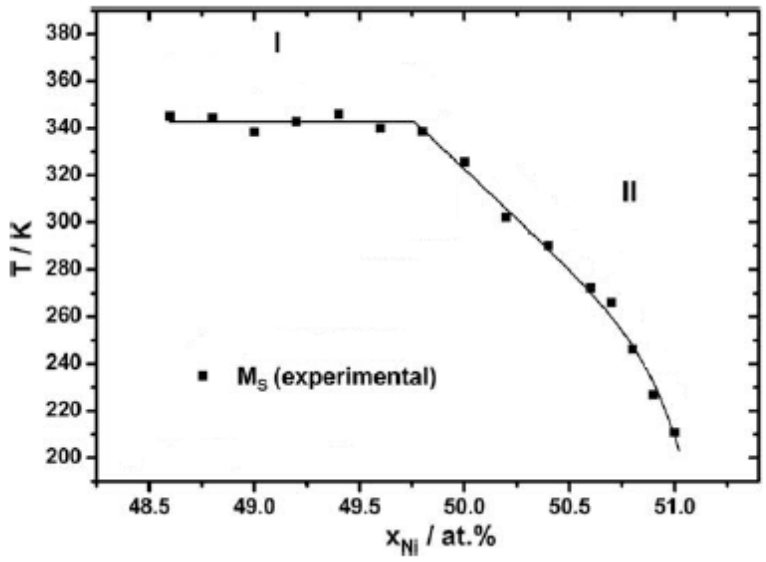

Figure 9: Influence of the Ni concentration (X_{Ni}) on the measured M_s temperature (Taken from [10]**, used without permission)**

The martensitic phase transformation for Ti-rich material is expected to occur above room temperature. Therefore, Ti-rich NiTi would be used for applications with operational conditions above room temperature. One example of such an application is NiTi thin films used as electrothermal microactuators [15].

2.3 Characterization of the Thermal-induced Phase Transformation

There are measurable changes during temperature cycling that can be used to characterize the thermal-induced phase transformation [10]. One of these is the change in lattice parameter of the crystal structure, as seen in Figure 2. The measurement used in this thesis is the latent heat of transformation. The latent heat of transformation is the energy to transform the shape memory

alloy from martensite to austenite or vice versa. This process is measured through calorimetry, which is the process of measuring the amount of heat absorbed or released during the solid-state phase transformation. Differential scanning calorimetry is used for the current thesis to measure the transformation temperatures of the material and will be described in more detail in the Materials and Methods Section.

Chapter 3
Background on Additive Manufacturing

Additive manufacturing (AM) as defined by the ASTM F42 Technical Committee is the “process of joining materials to make objects from three-dimensional (3D) model data, usually layer upon layer, as opposed to subtractive manufacturing methodologies” [16]. It is a near-net-shaping technology that allows for the direct fabrication of complex metallic parts and 3D geometries. AM is a manufacturing process where a structure is built by sequentially adding each layer of material in the desired shape specified by a computer-generated 3D model. Compared to traditional subtractive manufacturing methods, AM incurs much less waste and is more efficient [17]. Since there is no need for a mold, a prototype can be quickly manufactured and changes to a prototype can be made easily. For these reasons, AM has gained popularity as a manufacturing method. Although rapid prototyping has been available for some time and can be considered as AM with plastic materials, recent work has focused on fabricating metals [5].

According to ASTM classification, AM for metals can be categorized broadly into two groups: directed energy deposition and powder bed fusion [18]. Directed energy deposition is the method used for this thesis research. For both techniques, metallic powder is melted by an energy source.

In powder bed fusion, a bed of powder is spread over a build plate. A laser beam melts powder in the path of the beam using a scanner system, and the powder cools and solidifies. The powder delivery system then moves up and the build station piston retracts as the powder coater spreads a new layer of powder across the previous layer. This process is repeated layer by layer until the build is completed. This process is depicted in Figure 10 [18]. Powder bed fusion is limited by the horizontal layer construction and slow deposition rate, while directed energy deposition offers larger build envelopes and higher deposition rates [19].

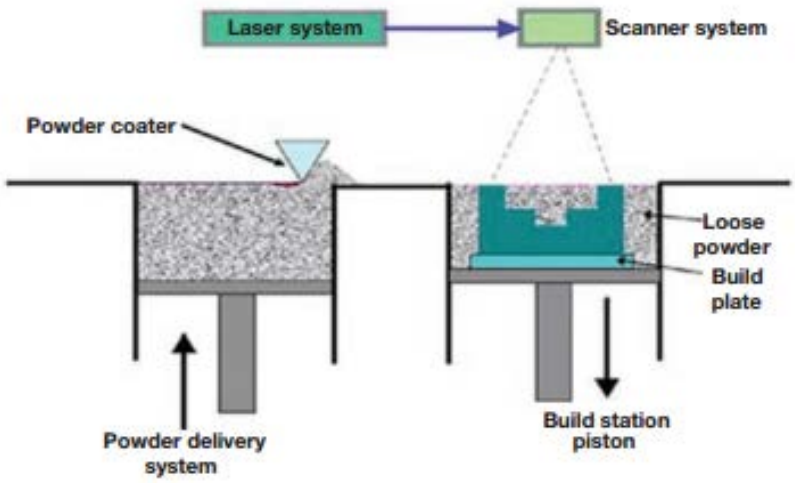

Figure 10: Schematic showing powder bed fusion technology (Taken from [18]**, used without permission)**

3.1 Directed Energy Deposition

For the AM technique directed energy deposition (DED) employed in this work, metallic powder feedstock flows into a meltpool with the flow directed by delivery nozzles [19]. To begin, powder travels through the nozzle to deliver the material into the meltpool. The cladding head's laser beam melts the material upon deposition. The delivery nozzles follow a path that is determined by the 3D model. As the nozzle moves, the meltpool just behind the nozzle solidifies

and the metal layer is formed. Layer by layer the part is built up onto the substrate to form the build coupon. This process is depicted in Figure 11 [19]. The hatch direction corresponds to the x-axis and the width of the build, the build direction is along the y-axis, and the z-axis corresponds to the build height [20].

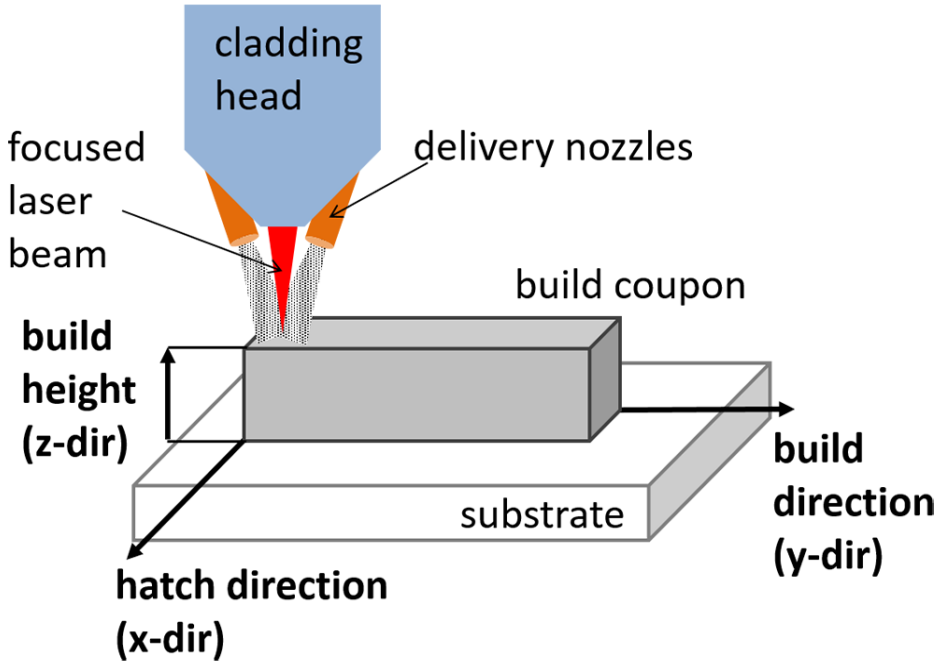

Figure 11: Schematic showing directed energy deposition (Taken from [20]**, used with authors' permission)**

3.2 AM of NiTi

As a fabrication approach for NiTi, AM is relatively new and is still being researched. Recent studies have shown the feasibility of using laser based AM with elementally blended Ni and Ti powders to fabricate NiTi SMAs [20-22]. One of the challenges with AM, however, is that it

brings about microstructure heterogeneity due to variations in feedstock distribution, thermal gradients, and residual stresses, which are all inherent to the fabrication process. As previously discussed, the layer-by-layer deposition process of AM can produce anisotropic properties [23-25]. In previous work from the Hamilton group, a spatial heterogeneity in the transformation temperatures was characterized for AM NiTi with large build volumes [10]. This spatial heterogeneity suggests an anisotropic microstructure. The following figure is from "Anisotropic Microstructure and Superelasticity of Additive Manufactured NiTi Alloy Bulk Builds Using Laser Directed Energy Deposition" by Bimber et. al., of the Hamilton group. The figure shows the microstructures of the as-deposited NiTi material observed at z-heights of 2.5mm, 6.0mm, and 8.5mm above the substrate. The heterogeneity in the microstructure can be seen in the differences between the three images as the distance from the substrate increases. At the 2.5mm distance, the Ni_3Ti phase appears globular, as shown in Figure 12 (c). With increasing build height, the globular Ni_3Ti phase is not observed, as shown in Figures 12 (a) and (b).

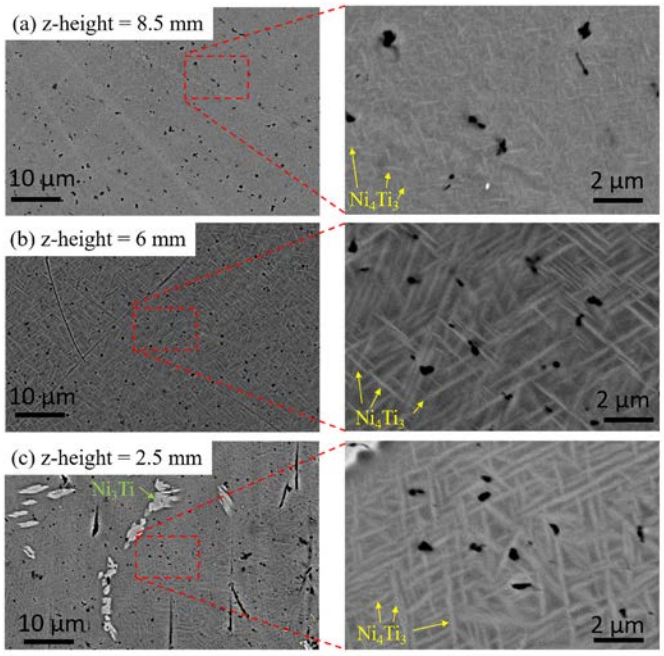

Figure 12: SEM images of the as-deposited compression specimen with a Ni-rich composition, which are at (a) 8.5 (b) 6, and (c) 2.5 mm z-heights . The Ni_4Ti_3 precipitate microstructure varies through the build height and thus the anisotropic microstructure exists for LDEDAM. For the Ti-rich material in this work, Ti_2Ni second phases are expected based on the phase diagram (see Fig 8). Though the presence of the Ti_2Ni phases is not confirmed in this work, an anisotropic microstructure of Ti_2Ni is expected to exist for Ti-rich alloys, as it is inherent to AM. (Taken from [6]**, used with authors' permission)**

This work confirms an anisotropic microstructure for the as-deposited builds of additively manufactured Ni-rich NiTi. [6].

This thesis research focuses on precipitation heat treatments for Ti-rich NiTi alloys. For the Ti-rich composition of this material, the phase diagram (Figure 8) shows that a solid-solution phase cannot be achieved and thus precipitation heat treatment is investigated. A high temperature very near the solidus temperature of 1275K (shown in Figure 8) was used for the heat treatments. Laser directed energy deposition AM (LDEDAM) is used to fabricate builds, and samples are micromachined from different spatial locations within the build. The samples are investigated using DSC to measure the thermal-induced phase transformation temperatures and enthalpies.

The degree to which measurements vary at different spatial locations is used to rationalize the effectiveness of the precipitation heat treatments for tailoring the transformation behavior of the AM NiTi builds.

Chapter 4
Materials and Methods

The material studied in this thesis is a Ti-rich NiTi alloy that was additively manufactured using the directed energy deposition technique. The specific details of this AM process are given in a recent publication by the Hamilton group [20]. For the DED AM process, elementally blended Ni and Ti powder feedstock was used. The powder blend ratio of Ni:Ti was 58:42 wt.% (46.9:53.1 at.%). The build parameters are given in Table 1.

Table 1: Specifications of AM process for build

Coupon ID:	B38
Feedstock (composition):	$Ni_{53}Ti_{47}$ wt.% for an equivalent composition of $Ni_{47.9}Ti_{53.1}$ at.% **(Ni-poor)**
Laser type and settings:	Nd:YAG laser, with 1 kW laser power
Laser travel speed: [in build direction (y-dir) in Fig. 11]	10.6 mm/s
Number of passes: [in hatch direction (x-dir) in Fig. 11]	6
Number of layers: [in build height (z-dir) in Fig. 11]	14
Substrate material:	Polished pure Ti

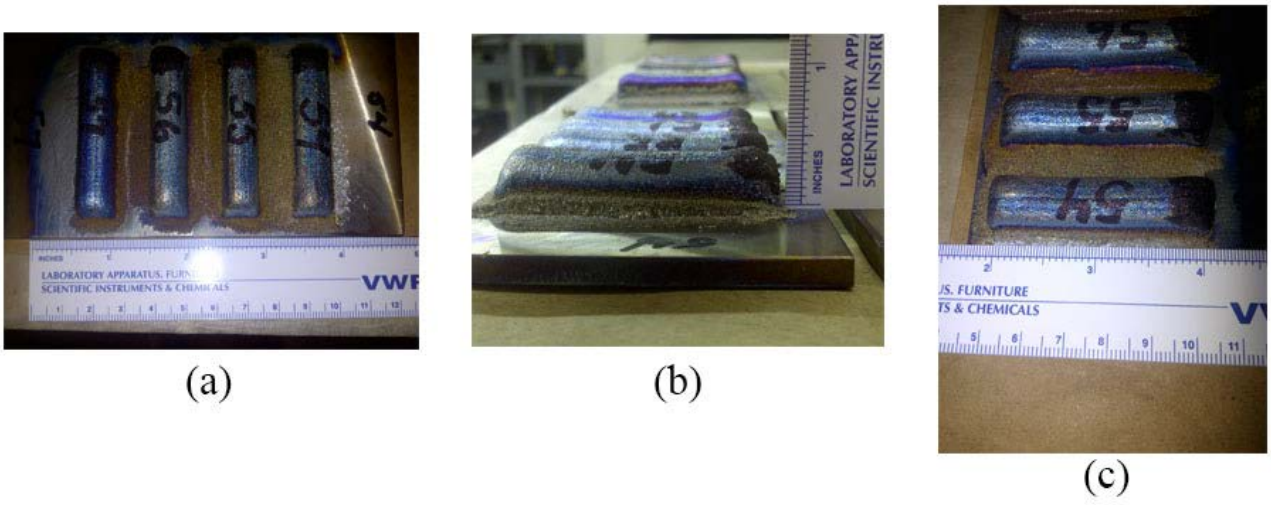

Figure 13: Images of the NiTi build coupons as-deposited onto the Ti-substrate showing (a) the width, (b) the height, and (c) the length of the as-deposited builds

The as-deposited build coupons are shown in Figure 13. The builds were deposited onto a heated (355°C) Ti-substrate and are shown adhered to the substrate. Compression specimens were extracted from these builds using wire electro-discharge machining (EDM). Figure 14 shows the specimen extraction locations along the build direction. The dimensions of the compression specimens were 4 mm by 4 mm, with an 8 mm length. The top surfaces were about 0.1 mm below the top layer of the build, and the bottom surfaces were about 0.2 mm above the substrate.

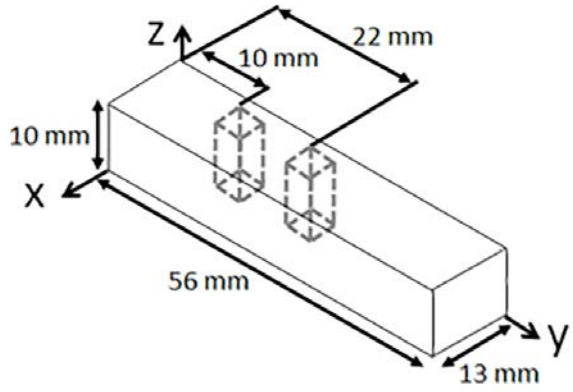

Figure 14: Extraction of compression specimens from the AM build (Taken from [6]**, used with authors' permission]**

4.1 Sample Preparation for this Work

The next step was to section compression specimens into small samples for differential scanning calorimetry (DSC) analysis. These DSC samples were extracted at the locations along the height of the compression specimens shown in Figure 15 using a slow speed diamond saw. The letters A-F correspond to the height location for each sample. Fig. 15 shows the height measurements for samples sectioned from the compression specimen micromachined from the as-deposited build.

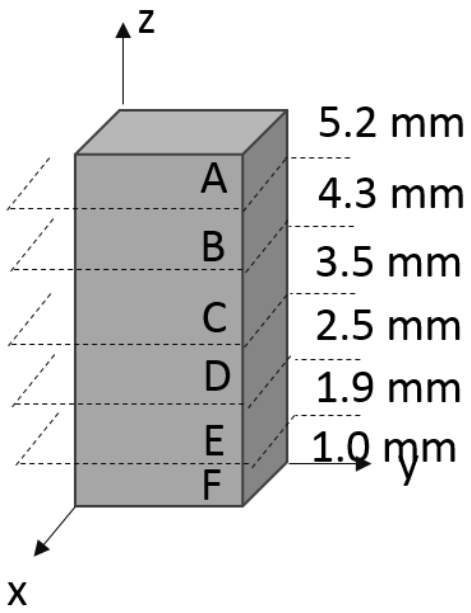

Figure 15: Locations for DSC specimen extraction along the build height.

4.2 Precipitation Heat Treatments

Precipitation heat treatments were carried out in a tube furnace in an inert Ar environment with a flow rate of ~1 L/min and were followed by a water quench (WQ). The furnace is located in Engineering Science and Mechanics Department's Center for Innovative Sintered Products (CISP). The heat treatment temperature (950 °C) was chosen to reach the temperature (1257 K) very near the solidus line (see Fig. 8) so that diffusion rates become appreciable to reduce the degree of anisotropy. This temperature and the durations (t >= 10 hours) are typical for Ni-rich NiTi alloys [6,26,27]. Other research on AM NiTi alloys used similar temperatures and times as well [5,21]. The first method attempted in this research was to heat treat the samples after sectioning them from the as-deposited material. Another method was to heat treat the

compression specimens before sectioning samples for DSC experiments. These two methods were chosen to highlight the difference between the effects of heat treating the compression specimens compared to heat treating the sectioned DSC samples. The heat treatment for the samples was 950 °C for 10 hours with WQ. For heat treating the compression specimens (prior to sectioning DSC samples), two heat treatments were employed: 950 °C for 10 hours with WQ, and 950 °C for 10 hours with WQ followed by another 950 °C heat treatment for 14 hours with WQ.

4.3 DSC Experimentation

The first step to characterize an SMA material is to establish the transformation temperatures: austenite start temperature (A_s), austenite finish temperature (A_f), martensite start temperature (M_s), and martensite finish temperature (M_f) without load applied. The temperatures can be determined using differential scanning calorimetry (DSC). DSC measures the changes in heat flow of a specimen with temperature over time [28]. While the temperature changes, the DSC measures a heat loss/gain against a reference sample. The specimen is enclosed in a pan and compared against an empty reference pan. The difference in thermal power required to maintain these both at the same temperature is measured and plotted in a thermogram. For determining the transformation temperatures, ASTM F2004 was followed [29], which is the standard for characterizing NiTi alloys using thermal analysis [29]. As stated in this standard, “this test method involves heating and cooling a test specimen at a controlled rate in a controlled environment through the temperature interval of the phase transformation” [29]. The program followed for this work had start and end conditions of 25°C and was as follows:

(i) Heat from 25°C to 125°C at 10°C/min

(ii) Hold for 1 minute at 125°C

(iii) Cool from 125°C to -120°C at 10°C/min

(iv) Hold for 1 minute at -120°C

(v) Heat from -120°C to 125°C at 10°C/min

The method was programmed using PerkinElmer Pyris software. The software outputs heat loss/gain and temperature data for plotting heat flow vs. temperature curves, also referred to as thermograms.

The transformation temperatures could be determined from the thermograms. An exothermic peak arises during cooling because heat is lost due to the forward phase transformation from austenite to martensite. An endothermic peak arises during heating as heat must be supplied to complete the reverse phase transformation from martensite back to austenite. The method of tangents, as described in ASTM F2004, was used to determine the A_s, A_f, M_f, and M_s temperatures for each experiment. The following figure depicts the method of tangents as it is used to obtain these measurements.

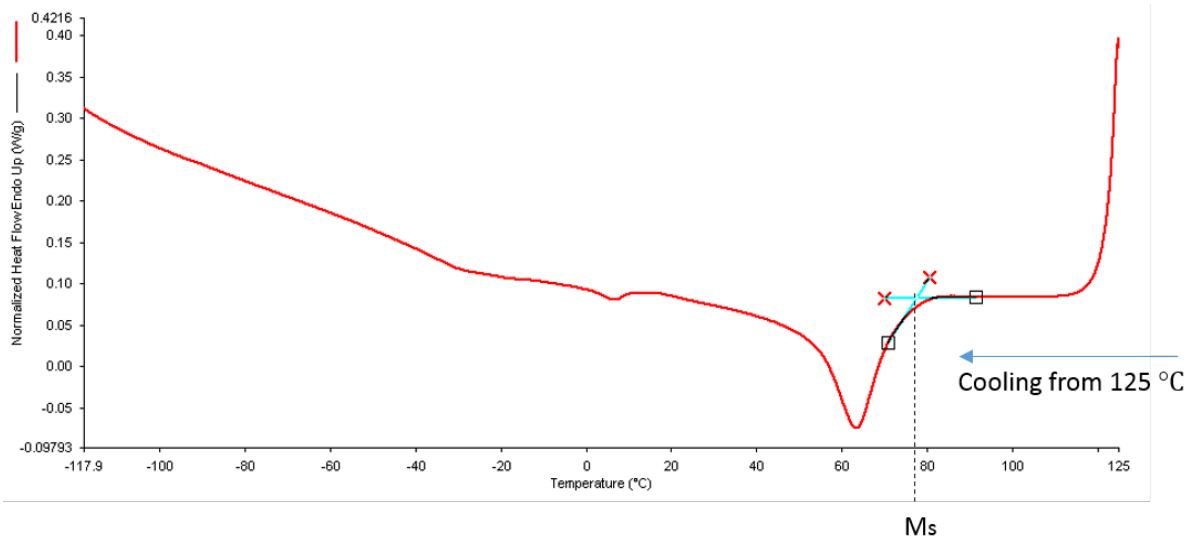

Figure 16: The method to determine transformation temperature measurements from the cooling segment of a heat flow vs. temperature curve

This figure shows how the M_s measurement is obtained for this example heating curve. The intersection of the two tangent lines corresponds to the temperature measurement. The transformation enthalpy was calculated from these DSC curves using the Pyris software, as depicted in the following figure. The blue shaded area corresponds to the “reverse” enthalpy and the red shaded area corresponds to the “forward” enthalpy.

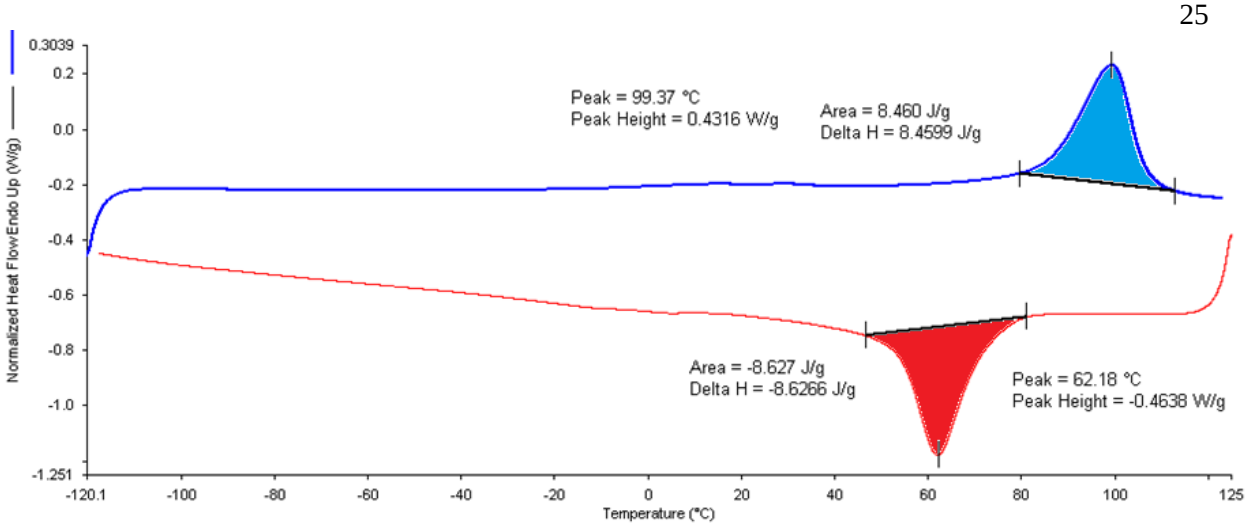

Figure 17: Complete heating and cooling DSC thermogram showing the area corresponding to enthalpy

Chapter 5
Results and Discussion

The AM Ti-rich NiTi material was studied in as-deposited and two heat treated conditions. A single stage heat treatment was 950°C for 10 hours and water-quench (WQ). A two stage heat treatment was 950°C for 10 hours WQ followed by 950°C for 14 hours WQ. For the single stage treatment, DSC samples were prepared using two approaches. For a sample treated approach, DSC samples were first sectioned from the compression specimen and subsequently given the single stage treatment. A specimen treatment approach started with heat treating the compression specimen using the single stage treatment and subsequently sectioning DSC samples from the heat treated specimen.

The first section in this chapter presents the DSC analysis for the as-deposited condition. The second section presents the analysis for the sample treatment approach with the single stage treatment. The last section presents the DSC analysis for the specimen treatment approach. In this section, the analysis for the single stage and two stage treatment conditions are presented. The DSC analysis of each condition is used to characterize the stress-free thermal-induced phase transformation with respect to transformation temperatures, peak temperatures, and/or transformation enthalpies.

5.1 As-deposited Condition

Figure 18(a) shows the cooling portion of the DSC thermograms for the as-deposited material and Figure 18(b) shows the heating portion. The specimens were sectioned from the as-deposited build through its z-height as shown in Figure 15. These specimens are labeled in Figure 18(a) (A-F), and each thermogram corresponds to a different DSC sample. Multiple peaks in each cooling curve in Figure 18(a) indicate that multiple exothermic reactions occur during the forward austenite-to-martensite phase transformation. The peaks closer to the substrate (at a smaller height) are less narrow than the peaks further away from the substrate for both the cooling portion and the heating portion.

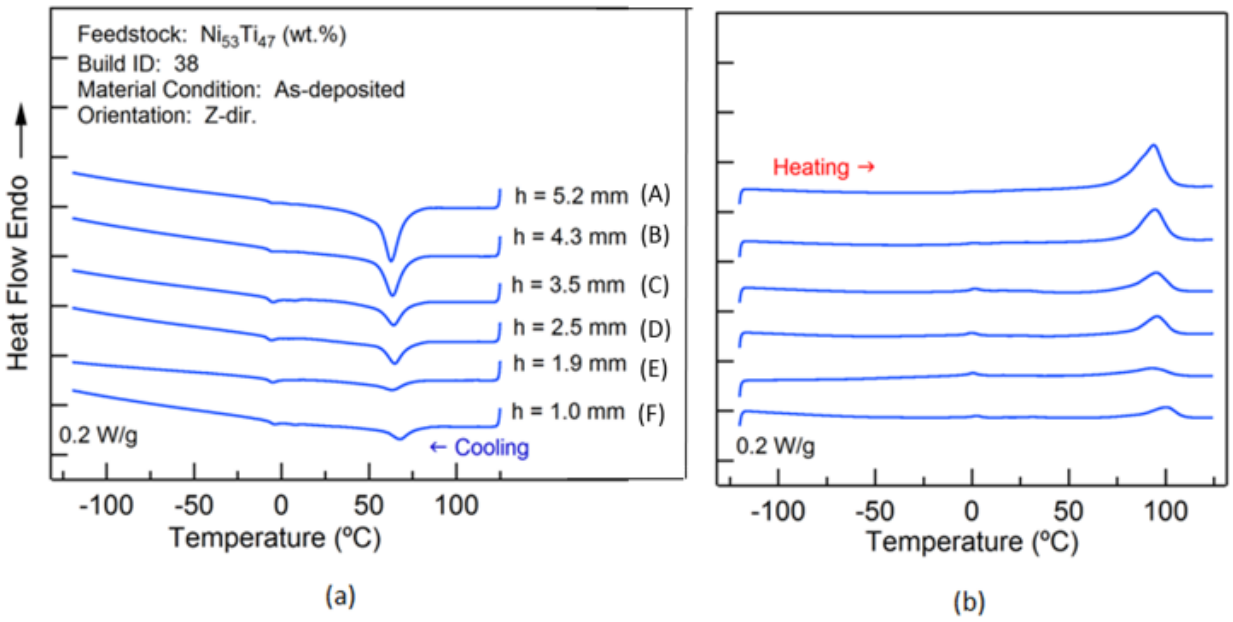

Figure 18: DSC thermogram for as-deposited material. (a) shows the cooling portion and (b) shows the heating portion.

The areas under these curves correspond to the enthalpies, (see Figure 19), which are plotted as a function of z-height. H_F is the enthalpy of the forward reaction, which is the area under the peaks

in the cooling portion of the DSC thermograms. H_R is the enthalpy of the reverse reaction, which is the area under the peaks in the heating portion. These enthalpy measurements show that the enthalpy is less for the specimens closer to the substrate. The enthalpies increase as the distance from the substrate increases, with the highest forward and reverse enthalpy measurements occurring furthest from the substrate (h=5.2mm). Figure 19 also shows that the forward and reverse enthalpies are not the same at each z-height, although they should be. This could be because there are small secondary peaks in the cooling portion that were not accounted for. The secondary peaks in the curves indicate multi-step phase transformations.

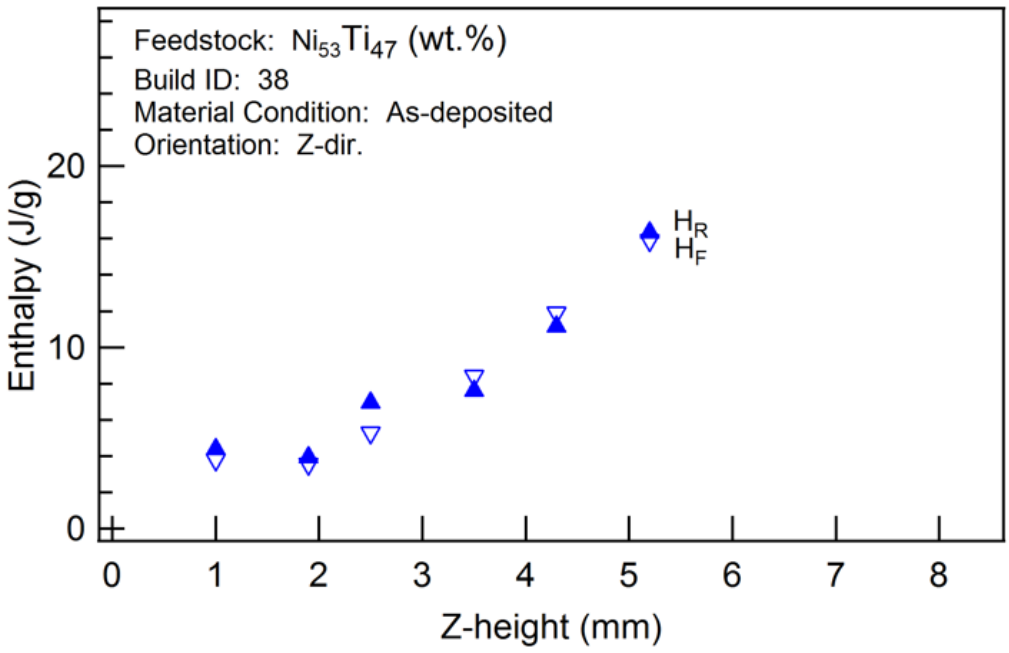

Figure 19: Enthalpies for the forward and reverse transformations for the as-deposited material

Figure 20(a) shows that the transformation and peak temperatures are different for the varying specimen heights. The M_s and M_p temperatures are highest closest to the substrate at h=1.00mm (F) and lowest furthest from the substrate at h=5.2mm (A). The A_{p1} temperature is highest closest to the substrate as well, and is equivalent for the rest of the heights. Figure 20(b) depicts the differences between the peak temperatures (A_p and M_p) at each z-height. This difference is largest closest to the substrate at h=1.00m (F) and the smallest at h=1.9mm (E). The difference between peak temperatures are equivalent further from the substrate, for h=3.5mm (C), h=4.3mm (B), and h=5.2mm (A).

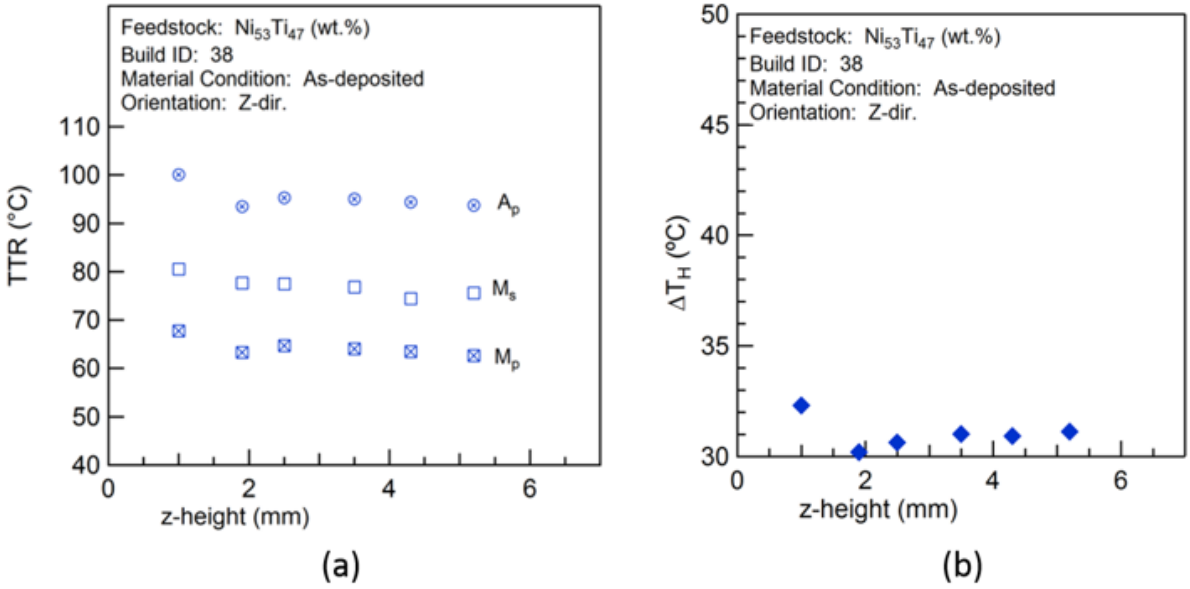

Figure 20: For the as-deposited material, (a) shows the transformation temperatures and (b) shows the difference between the peak temperatures

5.2 Sample Treatment Approach with Single Stage Treatment

For the sample treatment approach, the DSC thermograms are shown in Figure 21. The specimens were sectioned from the build, as labeled in the figure, and each thermogram corresponds to a different DSC sample. Multiple peaks in each cooling curve in Figure 21(a) indicate that multiple exothermic reactions occur during the forward austenite-to-martensite phase transformation. The number of exothermic peaks decreases from three (M_{p1}, M_{p2}, M_{p3}) to two (M_{p1}, M_{p2}) as the z-height increases. The height of M_{p1} increases as the distance from the substrate increases, with the highest peak at h=5.2mm (A). In Figure 21(b) there are multiple peaks in each heating curve which indicates that multiple endothermic reactions occur during the reverse martensite-to-austenite phase transformation. The number of peaks decreases from three to two with increasing distance from substrate. The height of A_{p1} increases with increasing distance from the substrate, with the highest peak at h=5.2mm (A). Comparing the cooling portion and heating portion of the thermograms, the M_{p1} and M_{p2} temperatures are much further apart than the A_{p2} and A_{p3} temperatures which are very close together.

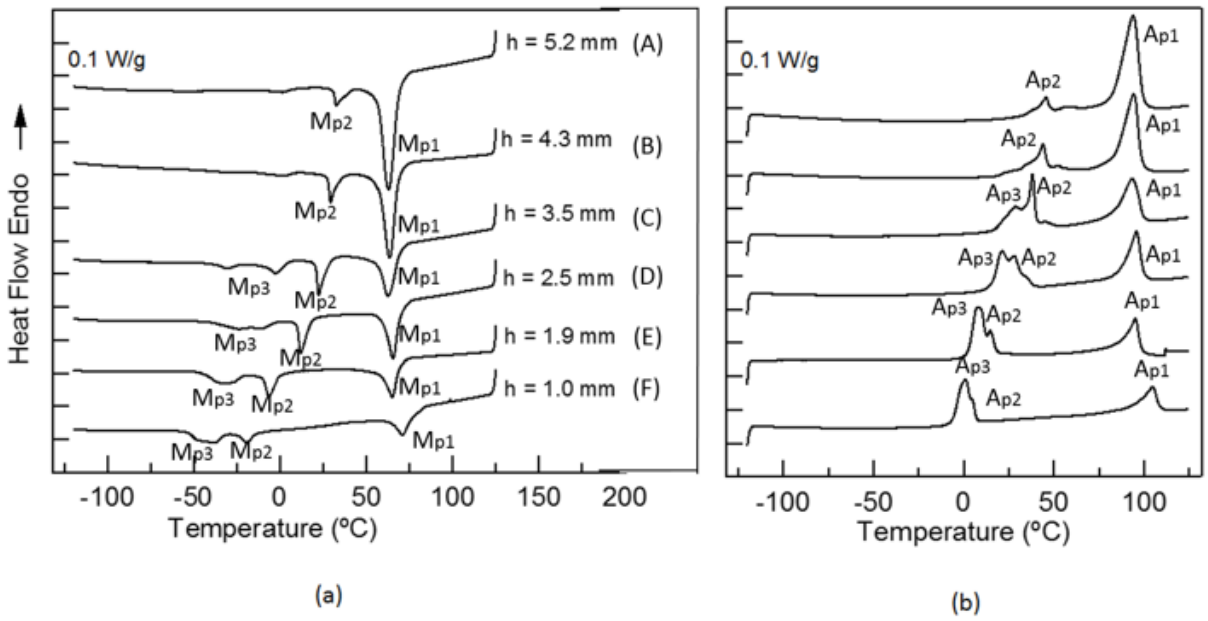

Figure 21: DSC thermogram for the single stage heat treatment. (a) shows the cooling portion and (b) shows the heating portion.

The transformation temperatures (M_s, M_p, and A_p) are shown in Figure 22. These transformation and peak temperatures are different for samples sectioned from different heights. The M_s and M_{p1} temperatures are highest closest to the substrate at h=1.00mm (F) and are equivalent for the other heights. The A_{p1} temperature is highest closest to the substrate and is equivalent for the other heights. The M_{p2}, M_{p3}, M_{p4}, A_{p2}, and A_{p3} temperatures rise with increasing z-height.

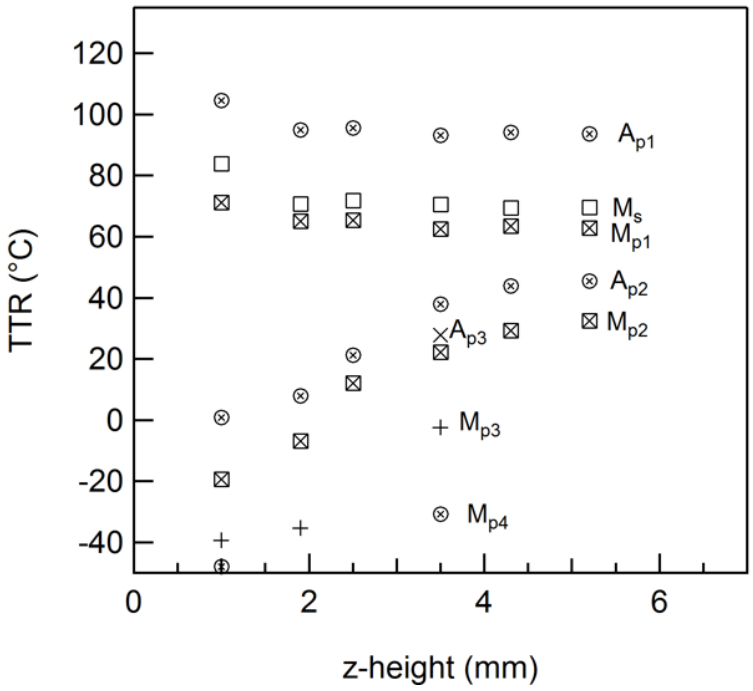

Figure 22: Transformation temperatures for the single stage heat treatment

5.3 Specimen Treatment Approach

5.3.1 Single Stage Heat Treatment

Figure 23(a) shows the cooling portion of the DSC thermogram for the single stage heat treatment material condition and Figure 23(b) shows the heating portion. The peaks closer to the substrate are again less narrow than the peaks further away from the substrate. The peaks are steeper for this material than they are for the as-deposited material. As they do for the as-deposited material, the height of the peaks increase with increasing distance from the substrate for both the exothermic peaks in Figure 23(a) and the endothermic peaks in Figure 23(b). Multiple peaks can be seen in the cooling and heating portions of the thermograms.

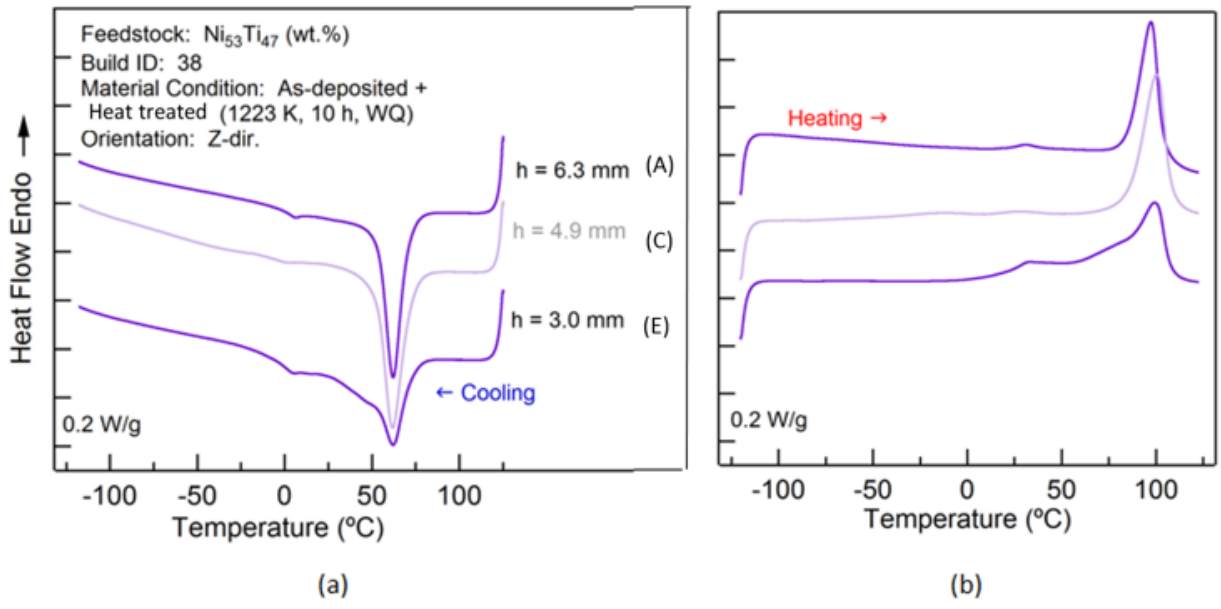

Figure 23: DSC Thermogram depicting the single stage heat treatment condition. (a) shows the cooling portion and (b) shows the heating portion.

Figure 24 shows the enthalpies of the forward and reverse reactions for the single stage treatment. The enthalpies of the reactions in the single stage treatment condition are larger than the enthalpies for the as-deposited material, in general. The forward and reverse enthalpies are not equal at each height, which indicates that the transformation is multi-step and may not be crystallographically reversible.

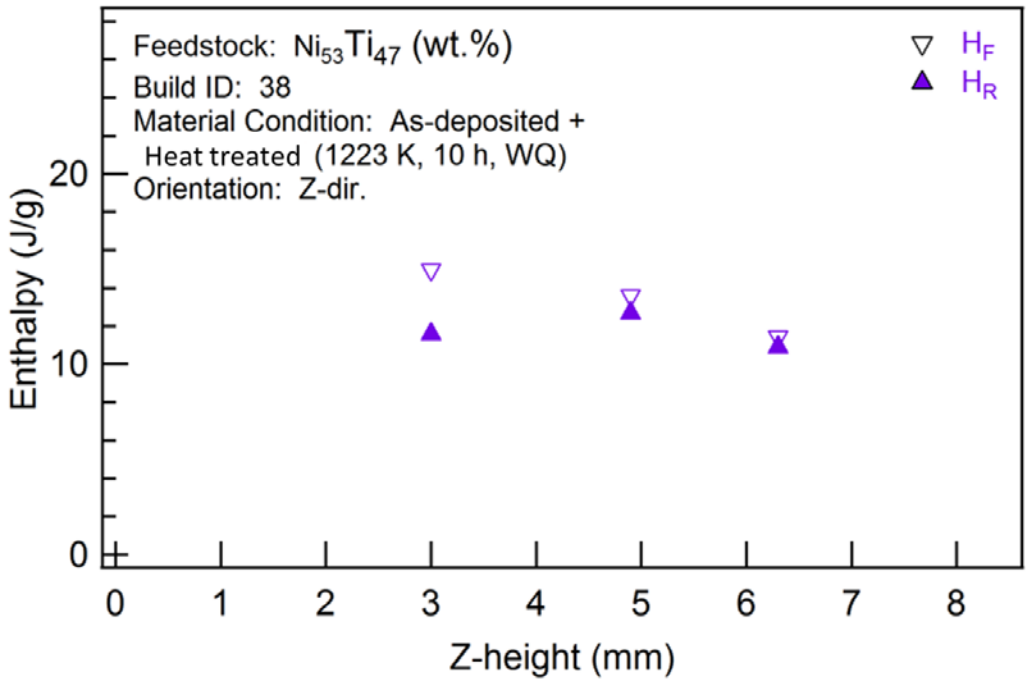

Figure 24: Forward and reverse enthalpies for single stage heat treatment condition

Figure 25(a) shows the transformation temperatures and Figure 25(b) shows the differences between the peak temperatures for the single stage treatment condition. The A_p and M_p temperatures are equivalent for the three different z-heights. The M_s temperatures decrease with increasing distance from the substrate, with the largest M_s temperature at h=3.0mm (E). The differences in peak temperatures varies for each z-height, with the largest difference in M_p and

A_p temperatures at h=4.9mm (C) and the smallest difference the furthest from the substrate at h=6.3mm (A).

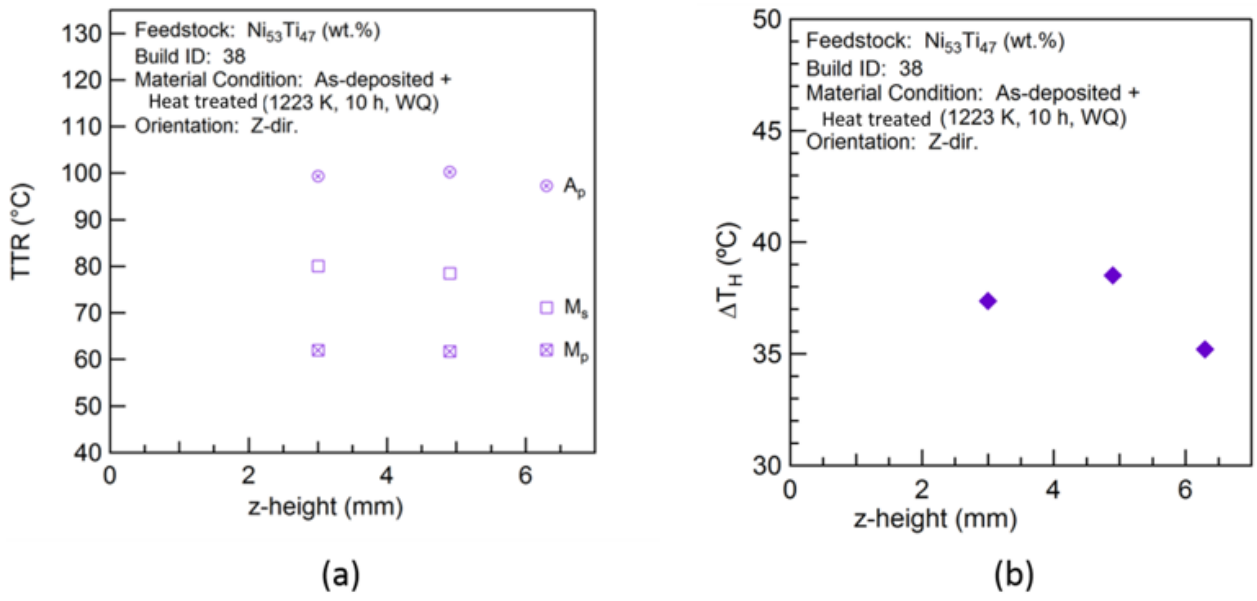

Figure 25: For the single stage heat treatment condition, (a) shows the transformation temperatures and (b) shows the differences between the peak temperatures

5.3.2 Two Stage Heat Treatment

Figure 26(a) shows the cooling portion of the DSC thermogram for the two stage heat treatment condition and Figure 26(b) shows the heating portion. The z-heights are labeled in Figure 26(a). The peaks closer to the substrate are less narrow than the peaks further away from the substrate for both the cooling portion and the heating portion. The highest exothermic peak and the highest endothermic peak both occur furthest from the substrate at h=4.4mm (E). The peaks are not as steep for this material as they were for the single stage heat treated material condition. Multiple peaks are visible in the DSC thermograms, which indicates a multi-stage transformation. These peaks appear smaller compared to the secondary peaks of the as-deposited or single stage heat treated materials.

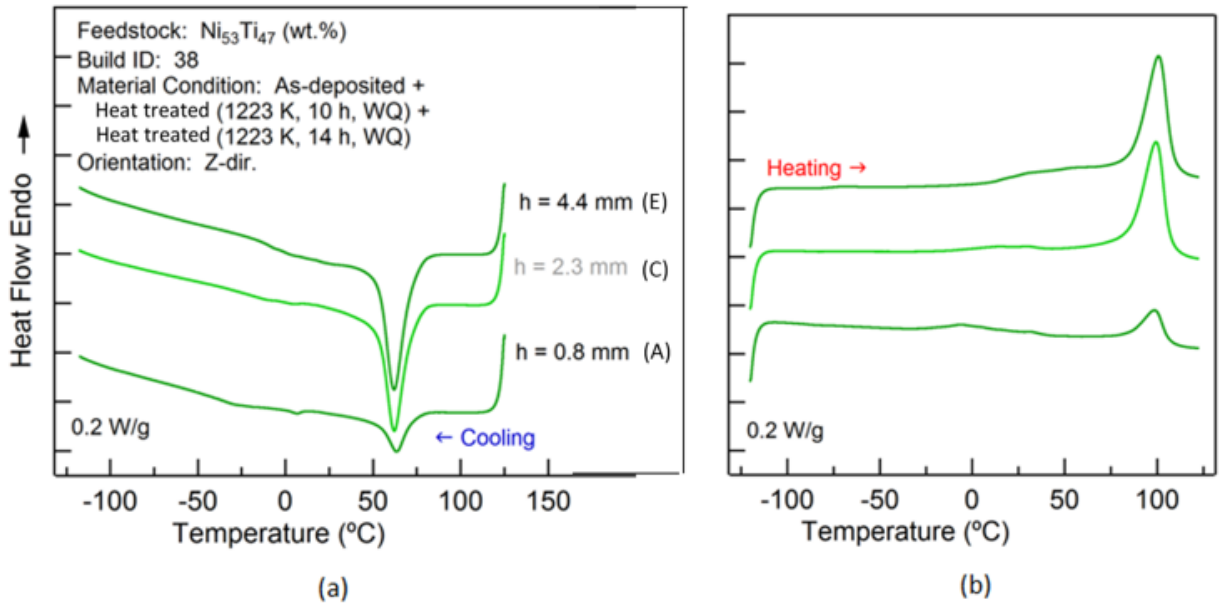

Figure 26: DSC thermogram depicting the two stage heat treatment condition. (a) shows the cooling portion and (b) shows the heating portion.

Figure 27 shows a plot of the enthalpies of the forward and reverse reactions for the two stage heat treated material. The enthalpies were closer in value to the as-deposited material than to the single stage heat treated material. The enthalpies for the forward and reverse reactions become equivalent with respect to those of the single stage heat treated material. The differences between the peak temperatures are also smaller for this material than the differences in peak temperatures for the single stage heat treated material. The forward and reverse enthalpies are largest the furthest from the substrate at h=4.4mm (E).

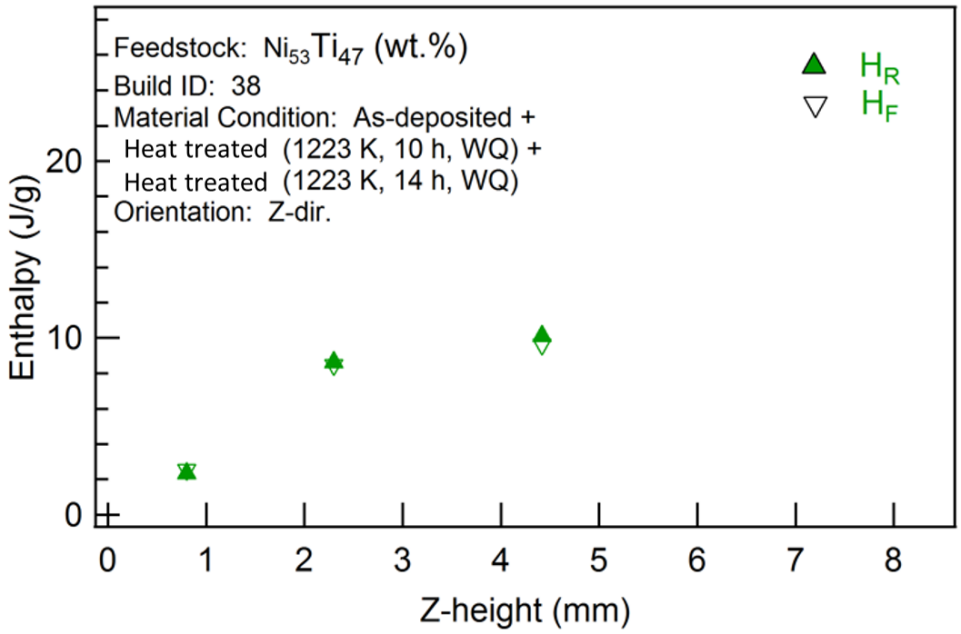

Figure 27: Forward and reverse enthalpies for the two stage heat treatment condition

Figure 28(a) shows the transformation temperatures and Figure 28(b) shows a plot of the differences between the peak temperatures for the two stage heat treated material. The A_p, M_p, and M_s temperatures are each equivalent over the varied z-heights. The difference in peak temperatures increases with increasing distance from the substrate.

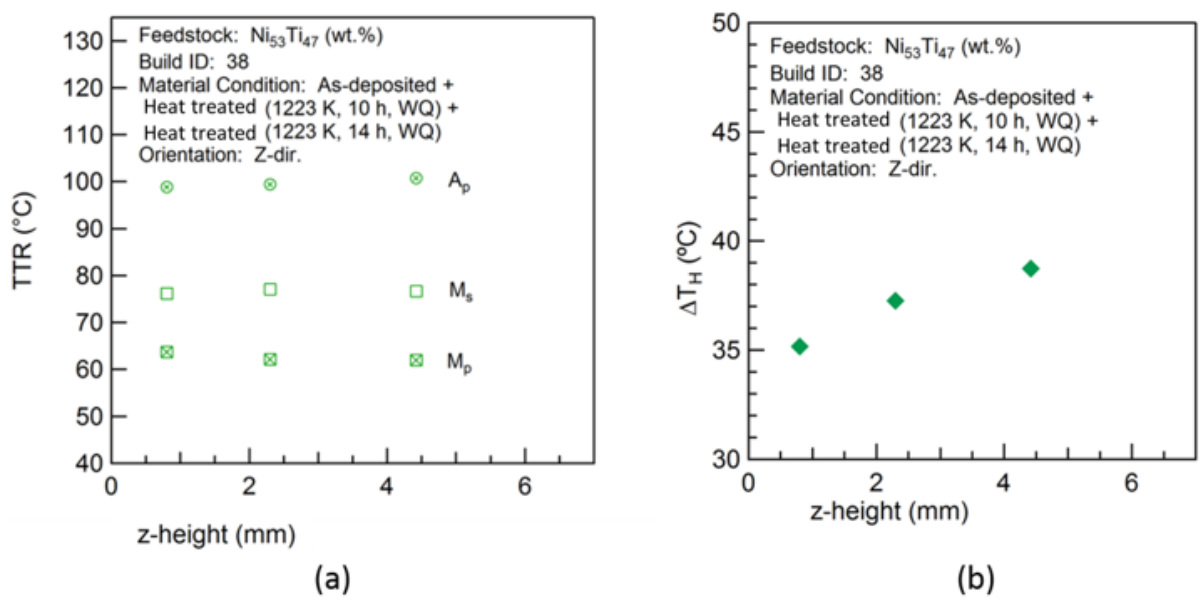

Figure 28: For the two stage heat treatment condition, (a) shows the transformation temperatures and (b) shows the differences between the peak temperatures

Chapter 6
Conclusions and Future Work

In summary, for laser directed energy deposition additive manufactured (LDEDAM) Ti-rich NiTi alloys, this work reports on the influence of precipitation heat treatments on the stress-free thermal-induced martensitic phase transformation (TIMT) temperatures. Elementally blended Ni and Ti powders were deposited with directed energy deposition in a ratio of 58:42 wt.% (46.9:53.1 at.%), which means the material was Ti-rich. The results of differential scanning calorimetry (DSC) analysis for two different durations for the same temperature are contrasted with those for the as-deposited condition. The influence of duration is reported in terms of the number of transformation events (peaks) that are obvious in the heat flow versus temperature curves (thermograms) obtained from DSC analysis. Measurements for the transformation temperatures, enthalpies, and hystereses taken from the thermograms are also contrasted. The analysis is conducted for DSC specimens extracted from different locations within a compression specimen, which was micromachined from an as-deposited LDEDAM Ti-rich NiTi alloy build coupon having a much larger size/volume than the compression specimen. Studying samples from different spatial locations provided insight into the differential behavior with respect to the build height, as an anisotropic microstructure is expected for material fabricated using AM.

A single stage heat treatment was used with two approaches for sample preparation: (1) the DSC samples were sectioned from the compression specimens and subsequently given the heat

treatment and (2) the compression specimen was heat treated and DSC samples were sectioned from the heat treated compression specimen. Multiple transformation peaks existed in the DSC curves for the samples prepared using approach 1 (referred to as “sample treatment”) in stark contrast to the major peak observed for the as-deposited material. For samples prepared using approach 2 (referred to as “specimen treatment”), the number of peaks in the thermograms was equivalent to the as-deposited condition. The transformation temperatures for the sample treatment changed, markedly with height; whereas, by comparison, the temperatures were equivalent for the specimen treatment. From this phase of the work, we draw the conclusion that diffusion plays a vital role. Consequently, a longer duration two-step precipitation heat treatment was explored only using approach 2 (the specimen treatment).

The following conclusions can be drawn:

- The M_s temperatures were most consistent between the different heights for the two-step treatment.
- The precipitation heat treatments created “steeper” curves in the DSC thermograms, which suggests that a larger volume fraction of material underwent the transformation at a similar driving force.
- Secondary peaks in the DSC thermograms indicate a multistage thermal-induced phase transformation in the microstructure, which may be related to the transformation path differing locally in material influenced by the Ti_2Ni secondary phase.
- The longer duration precipitation heat treatment reduced the size of the secondary peaks.

The results from DSC analysis show that the transformation temperatures for the precipitation heat-treated material are comparable to the as-deposited material. The enthalpy measurements

for the TIMT on cooling and heating become equivalent for the longer duration precipitation heat treatment.

Future work on heat treatments needs to be done on as-deposited build coupons. Microstructure characterization with different post-deposition heat treatments should be included to see how the microstructure behaves. Ultimately, the results show that precipitation treatments may improve the reversibility of the TIMT without altering the operating temperature ranges. Future work on the shape memory effect and psuedoelastic effect response would confirm improved reversibility and performance for practical applications that can take advantage of shape memory behavior.

Appendix
Transformation Temperatures

The transformation temperatures in the tables below correspond to the plots in the results section of this thesis. The “heights” are the z-heights on the x-axis of the plots. M_s is the martensite start temperature, M_p is the martensite peak temperature, A_p is the austenite start temperature, H_f is the enthalpy for the forward transformation, H_r is the enthalpy for the reverse transformation, and ΔT_h is the difference in peak temperatures. For Table 2, multiple peak temperatures are given since there were multiple visible peaks in some of the curves on the thermogram for this material (see Figure 21). The following figure is of a thermogram that has been labeled with the transformation temperatures and enthalpies.

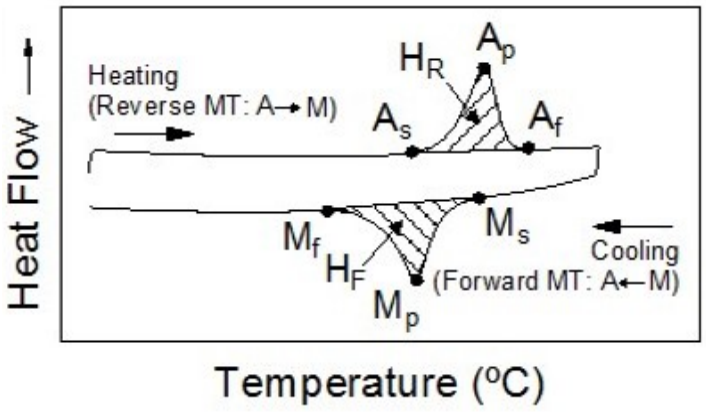

Figure 29: Labeled thermogram showing the transformation temperatures

Table 2: Transformation temperatures for the sample treatment approach with single stage heat treatment

Sample ID	Height (mm)	Ms (°C)	Mp1 (°C)	Mp2 (°C)	Mp3 (°C)	Mp4 (°C)	Ap1 (°C)	Ap2 (°C)	Ap3 (°C)
B38C6ASL	5.2	69.7	62.97	32.52			93.74	45.59	
B38C6BSL	4.3	69.4	63.5	29.27			94.18	43.95	
B38C6CSL	3.5	70.64	62.6	22.32	-2.41	-30.75	93.31	38	27.84
B38C6DSL	2.5	71.94	65.48	12.07			95.67	21.3	28.38
B38C6ESL	1.9	70.77	65.15	-6.88	-35.4		95.06	7.93	14.9
B38C6FSL	1	83.9	71.2	-19.4	-39.33	-47.94	104.67	0.86	

Table 3: Transformation temperatures for the as-deposited material

Sample ID	Height (mm)	Ms (°C)	Mp (°C)	Ap (°C)	Hf (J/g)	Hr (J/g)	ΔT_h (°C)
B38C6A	5.2	75.64	62.64	93.77	15.8835	16.3289	31.13
B38C6B	4.3	74.45	63.5	94.42	11.8846	11.1507	30.92
B38C6C	3.5	76.86	64.1	95.12	8.415	7.5967	31.02
B38C6D	2.5	77.49	64.74	95.37	5.2676	6.9438	30.63
B38C6E	1.9	77.69	63.35	93.55	3.5591	3.9301	30.2
B38C6F	1	80.57	67.78	100.1	3.7832	4.3765	32.32

Table 4: Transformation temperatures for the section treatment approach – single stage heat treatment

Sample ID	Height (mm)	Ms (°C)	Mp (°C)	Ap (°C)	Hf (J/g)	Hr (J/g)	ΔT_h (°C)
B382C4SLA	6.3	72.21	62.11	97.31	11.4358	10.9132	35.2
B382C4SLC	4.9	78.49	61.8	100.31	13.5976	12.6705	48.46
B382C4SLE	3	80.07	62.02	99.39	14.955	11.5793	37.37

Table 5: Transformation temperatures for the section treatment approach – two stage heat treatment

Sample ID	Height (mm)	Ms (°C)	Mp (°C)	Ap (°C)	Hf (J/g)	Hr (J/g)	ΔT_h (°C)
B38C8SLA	0.8	76.24	63.72	98.89	2.3411	2.5582	35.17
B38C8SLC	2.3	77.14	62.18	99.45	8.6266	8.4599	37.27
B38C8SLE	4.4	76.67	62.03	100.76	10.0987	9.6432	38.73

Bibliography

[1] J. Mohd Jani, M. Leary, A. Subic, and M. A. Gibson, “A review of shape memory alloy research, applications and opportunities,” *Mater. Des.*, vol. 56, pp. 1078–1113, 2014.

[2] M. H. Wu and L. M. Schetky, “Industrial Applications for Shape Memory Alloys,” *Int. Conf. Shape Mem. Superelastic Technolgies*, vol. 182, pp. 171–182, 2000.

[3] P. A. Besselink, “Recent Developments on Shape Memory Applications,” *J. Phys. IV*, vol. 7, no. 1 997, pp. C5–581, 1997.

[4] A. P. Markopoulos, I. S. Pressas, and D. E. Manolakos, “A review on the machining of nickel-titanium shape-memory alloy,” *Rev. Adv. Mater. Sci.*, vol. 42, pp. 28–35, 2015.

[5] C. Haberland, M. Elahinia, J. Walker, H. Meier, and J. Frenzel, “Additive Manufacturing of Shape Memory Devices and Pseudoelastic Components,” in *ASME 2013 Conference on Smart Materials, Adaptive Structures and Intelligent Systems*, 2013, vol. 1, no. 1, pp. 1–8.

[6] B. A. Bimber, R. F. Hamilton, J. Keist, and T. A. Palmer, “Anisotropic Microstructure and Superelasticity of Additive Manufactured NiTi Alloy Bulk Builds Using Laser Directed Energy Deposition,” *manuscrupt*, 2016.

[7] N. Sharma, K. K. Jangra, and T. Ra1, “Fabrication of NiTi alloy: A review,” *Proc. Inst. Mech. Eng. Part B J. Eng. Manuf.*, vol. 229, no. 8, pp. 1273–1288, 2015.

[8] B. Donohue, “Developing a good memory: Nitinol shape memory alloy,” *Today’s Mach. World*, vol. 5, pp. 43–48, 2009.

[9] K. Otsuka and X. Ren, “Physical metallurgy of Ti-Ni-based shape memory alloys,” *Prog. Mater. Sci.*, vol. 50, no. 5, pp. 511–678, 2005.

[10] J. Frenzel, E. P. George, A. Dlouhy, C. Somsen, M. F.-X. Wagner, and G. Eggeler, “Influence of Ni on martensitic phase transformations in NiTi shape memory alloys,” *Acta Mater.*, vol. 58, no. 9, pp. 3444–3458, 2010.

[11] T. Duerig, a Pelton, and D. Stöckel, “An overview of nitinol medical applications,” *Mater. Sci. Eng. A*, vol. 273–275, pp. 149–160, 1999.

[12] D. C. Lagoudas, J. Boyd, D. Hartl, and I. Karaman, “Definition of a Shape Memory Alloy,” *Texas A&M SmartLab*. [Online]. Available:

http://smart.tamu.edu/overview/smaintro/simple/definition.html. [Accessed: 07-Mar-2016].

[13] P. K. Kumar and D. C. Lagoudas, *Introduction to Shape Memory Alloys*, vol. 1. 2008.

[14] J. Ryhänen, *Biocompatibility Evaluation of Nickel- Titanium Shape Memory Metal Alloy of Nickel-Titanium Shape*, vol. 41, no. 3. 1999.

[15] N. Frantz, E. Dufour-Gergam, J. P. Grandchamp, a. Bosseboeuf, W. Seiler, G. Nouet, and G. Catillon, "Shape memory thin films with transition above room temperature from Ni-rich NiTi films," *Sensors Actuators, A Phys.*, vol. 99, no. 1–2, pp. 59–63, 2002.

[16] N. Guo and M. C. Leu, "Additive manufacturing: Technology, applications and research needs," *Front. Mech. Eng.*, vol. 8, no. 3, pp. 215–243, 2013.

[17] D. Thomas and S. Gilvert, "Costs and Cost Effectiveness of Additive Manufacturing," *US Dep. Commer.*, no. December, 2014.

[18] B. Dutta and F. H. (Sam) Froes, *The additive manufacturing (AM) of titanium alloys*. Elsevier Inc., 2015.

[19] F. H. Froes and B. Dutta, "Additive Manufacturing of Titanium Alloys," *Adv. Mater. Res.*, vol. 1019, no. February, pp. 19–25, 2014.

[20] R. F. Hamilton, T. A. Palmer, and B. A. Bimber, "Spatial characterization of the thermal-induced phase transformation throughout as-deposited additive manufactured NiTi bulk builds," *Scr. Mater.*, vol. 101, pp. 56–59, Feb. 2015.

[21] P. R. Halani and Y. C. Shin, "In Situ Synthesis and Characterization of Shape Memory Alloy Nitinol by Laser Direct Deposition," *Metall. Mater. Trans. A*, vol. 43, no. 2, pp. 650–657, Sep. 2012.

[22] P. R. Halani, I. Kaya, Y. C. Shin, and H. E. Karaca, "Phase transformation characteristics and mechanical characterization of nitinol synthesized by laser direct deposition," *Mater. Sci. Eng. A*, vol. 559, pp. 836–843, Jan. 2012.

[23] T. Bormann, R. Schumacher, B. Müller, M. Mertmann, and M. de Wild, "Tailoring Selective Laser Melting Process Parameters for NiTi Implants," *J. Mater. Eng. Perform.*, vol. 21, no. 12, pp. 2519–2524, Jul. 2012.

[24] B. E. Carroll, T. a. Palmer, and A. M. Beese, "Anisotropic tensile behavior of Ti-6Al-4V components fabricated with directed energy deposition additive manufacturing," *Acta Mater.*, vol. 87, pp. 309–320, 2015.

[25] X. Zhou, K. Li, D. Zhang, X. Liu, J. Ma, W. Liu, and Z. Shen, “Textures formed in a CoCrMo alloy by selective laser melting,” *J. Alloys Compd.*, vol. 631, pp. 153–164, 2015.

[26] Y. Liu and P. G. McCormick, “Influence of heat treatment on the mechanical behaviour of a NiTi alloy.,” *ISIJ Int.*, vol. 29, no. 5, pp. 417–422, 1989.

[27] H. Sehitoglu, R. Hamilton, D. Canadinc, X. Y. Zhang, K. Gall, I. Karaman, Y. Chumlyakov, and H. J. Maier, “Detwinning in NiTi alloys,” *Metall. Mater. Trans. A*, vol. 34, no. 1, pp. 5–13, 2003.

[28] P. Gill, T. T. Moghadam, and B. Ranjbar, “Differential scanning calorimetry techniques: applications in biology and nanoscience.,” *J. Biomol. Tech.*, vol. 21, no. 4, pp. 167–193, 2010.

[29] ASTM, “ASTM F2004: Standard Test Method for Transformation Temperature of Nickel-Titanium Alloys by Thermal Analysis,” vol. 05, no. Reapproved 2010. pp. 1–4, 2004.

[30] C. Haberland, J. Frenzel, and H. Meier, “On the Properties of Ni-Rich NiTi Shape Memory Parts Produced by Selective Laser Melting,” in *Conference On Smart Materials, Adaptive Structures and Intelligent Systems*, 2012, pp. 1–8.

ACADEMIC VITA

Jessica Spoll
jessicaspoll@gmail.com

EDUCATION:

Bachelor of Science, Engineering Science
Minor in Mathematics
The Pennsylvania State University - Schreyer Honors College
Dean's List: Fa12, Sp13, Sp14, Fa14, Sp15, Fa15

EXPERIENCE:

Product Architecture Engineering Intern
May – August 2015
Volvo Construction Equipment, Braås, Sweden
- Analyzed parts and systems to create a new modular structure across product platforms
- Presented a new initiative to senior management
- Researched and wrote product feasibility plans

Mechanical Engineering Independent Research
August 2014 – May 2015
The Pennsylvania State University, University Park, PA
- Designed an experiment to determine the cutting force exerted by scalpel blades on tissue
- Modeled the relationship between a scalpel blade's edge-geometry and the force it exerts

Toshiba - Westinghouse Engineering Fellows Program
May – August 2014
The Pennsylvania State University, University Park, PA
- Proved the concept of a robotic navigation system for dry cask storage of used nuclear fuel
- Built and programmed a robot to traverse the difficult geometry of an inlet vent

Mechanical Engineering Research Intern
May - August 2013
Washington State University, Pullman, WA
- Programmed an application for SolidWorks to estimate disassembly time of product designs
- Created SolidWorks models for case studies ~ 100+ hours
- Published a paper in ASME's Journal of Computational Science

LEADERSHIP:

Project Manager, Technology Captain for THON (‘15-current)

- Lead a team of developers to rebuild THON’s volunteer website on a new framework
- Serve as the liaison between THON’s executive directors and my team of developers

Ambassador, Engineering Ambassadors (‘14-current)

- Create and deliver outreach presentations to promote interest in STEM
- Give tours of Penn State’s College of Engineering to prospective students
- Develop advanced communication and leadership skills

Teaching Assistant, Technical Writing for Engineers (‘15-current)

- Revise and review students’ technical reports
- Lead critique workshops

Teaching Assistant, Effective Speech for Engineers (‘14-current)

- Design and lead class activities to improve the communication skills of engineering students
- Prepare and present example speeches

HONORS:

Honorable Mention, Joelle Award for Women in Engineering Leadership (‘15)
Member, Tau Beta Pi – Engineering Honors Society (‘15)
Finalist, Leonhard Center Speaking Contest (‘14)
Recipient, Riegel Honors Scholarship for Women in Engineering (‘15)
Recipient, Longenecker and Associates Scholarship in Engineering Science (‘14)
Recipient, Richard P. McNitt Scholarship in Engineering Science (‘14, ‘15)
Recipient, The President’s Freshman Award (‘13)

SKILLS:

C++, Python, Django, MATLAB, PHP, SQL, SolidWorks, Arduino, HTML, CSS, Adobe Photoshop, PowerPoint, Excel, Access, R

PUBLICATIONS:

Hu Y, Srinivasan R, Spoll J, Ameta G. Graph Based Method and Tool for Complete and Selective Disassembly Time Estimation in Early Design. ASME. *J. Comput. Inf. Sci. Eng.* 2015;15(3):031005-031005-10. doi:10.1115/1.4029752.